Recording, Modeling and Visualization of Cultural Heritage, Ascona, Switzerland, May 22-27, 2005, pp.115-126.
http://www.photogrammetry.ethz.ch/general/persons/devrim_publ.html

Registration of point clouds using range and intensity information

D. Akca
Institute of Geodesy and Photogrammetry, ETH Zurich, Switzerland

ABSTRACT: An algorithm for the least squares matching of overlapping 3D surfaces is presented. It estimates the transformation parameters between two or more fully 3D surfaces, using the Generalized Gauss-Markoff model, minimizing the sum of squares of the Euclidean distances between the surfaces. This formulation gives the opportunity of matching arbitrarily oriented 3D surfaces simultaneously, without using explicit tie points. Besides the mathematical model and execution aspects we give further extensions of the basic model: simultaneous matching of multi sub-surface patches, and matching of surface geometry and its attribute information, e.g. reflectance, color, temperature, etc. under a combined estimation model. We give practical examples for the demonstration of the basic method and the extensions.

1 INTRODUCTION

For 3D object modeling data acquisition must be performed from different standpoints. The derived local point clouds must be transformed into a common system. This procedure is usually referred to as registration. In the past, several efforts have been made concerning the registration of 3D point clouds. One of the most popular methods is the Iterative Closest Point (ICP) algorithm developed by Besl & McKay (1992), Chen & Medioni (1992), and Zhang (1994). The ICP is based on the search of pairs of nearest points in the two sets and estimates the rigid body transformation, which aligns them. Then, the rigid body transformation is applied to the points of one set and the procedure is iterated until convergence.

Several variations and improvements of the ICP method have been made (Bergevin et al. 1996, Masuda & Yokoya 1995). In Besl & McKay (1992) and Zhang's (1994) works the ICP requires every point in one surface to have a corresponding point on the other surface. An alternative approach to this search scheme was proposed by Chen & Medioni (1992). They used the distance between the surfaces in the direction normal to the first surface as a registration evaluation function instead of the point–to–nearest point distance. This point-to-tangent plane distance idea was originally proposed by Potmesil (1983). In Dorai et al. (1997) the method of Chen & Medioni was extended to an optimal weighted least-squares framework. Zhang (1994) proposed a thresholding technique using robust statistics to limit the maximum distance between points. Masuda & Yokoya (1995) used the ICP with random sampling and least median square error measurement that is robust to a partially overlapping scene. Okatani & Deguchi (2002) proposed the best transformation of two range images to align each other by taking into account the measurement error properties, which are mainly dependent on both the viewing direction and the distance to the object surface.

The ICP algorithm always converges monotonically to a local minimum with respect to the mean-square distance objective function (Besl & McKay 1992). It does not use the local surface gradients in order to direct the solution to a minimum. Several reviews and comparison studies about the ICP variant methods are available in the literature (Jokinen & Haggren 1998, Williams et al. 1999, Campbell & Flynn 2001, Rusinkiewicz & Levoy 2001).

In Szeliski & Lavallee (1996) and Neugebauer (1997) two gradient descent type of algorithms were given. They adopt the Levenberg-Marquardt method for the estimation.

Since 3D point clouds derived by any method or device represent an object surface, the problem should be defined as a surface matching problem. In Photogrammetry, the problem statement of surface patch matching and its solution method was first addressed by Gruen (1985) as a straight extension of Least Squares Matching (LSM).

There have been some studies on the absolute orientation of stereo models using Digital Elevation Models (DEM) as control information (Ebner & Strunz 1988, Rosenholm & Torlegard 1988). This work is known as DEM matching. This method basically estimates the 3D similarity transformation parameters between two DEM patches, minimizing the sum of squares of differences along the z-axes.

Maas (2002) successfully applied a similar method to register airborne laser scanner strips, among which vertical and horizontal discrepancies generally show up due to GPS/INS inaccuracy problems. Another similar method has been presented in Postolov et al. (1999) for registering surfaces acquired using different methods, in particular, laser altimetry and photogrammetry. Furthermore, techniques for 2.5D DEM surface matching have been developed, which correspond mathematically to Least Squares Image Matching. The DEM matching concept can only be applied to 2.5D surfaces, whose analytic function is described in the explicit form as a single valued function, i.e. $z=f(x,y)$. 2.5D surfaces are of limited value in case of generally formed objects.

When the surface curvature is either homogeneous or isotropic, as it is the case with all first or second order surfaces, e.g. plane or sphere, the geometry-based registration techniques will fail. In some studies surface geometry and intensity (or color) information has been combined in order to solve this problem. Maas (2002) used the airborne laser scanner reflectance images as complimentary to the height data for the determination of horizontal shift parameters between the laser scanner strips of flat areas. Roth (1999) and Vanden Wyngaerd & Van Gool (2003) used feature-based methods in which interest points and regions are extracted from the intensity images. More often the intensity information is processed as a metric under an ICP algorithm in order to reduce the search effort of correspondent point pairs or in order to eliminate the ambiguities due to inadequate geometric information on the object surface (Weik 1997, Johnson & Kang 1999, Godin et al. 2001, Yoshida & Saito 2002).

The LSM (Gruen 1985) concept has been applied to many different types of measurement and feature extraction problems due to its high level of flexibility and its powerful mathematical model: Adaptive Least Squares Image Matching, Geometrically Constrained Multiphoto Matching, Image Edge Matching, Multiple Patch Matching with 2D images, Multiple Cuboid (voxel) Matching with 3D images, Globally Enforced Least Squares Template Matching, Least Squares B-spline Snakes. For a detailed survey the author refers to Gruen (1996). If 3D point clouds derived by any device or method represent an object surface, the problem should be defined as a surface matching problem instead of a point cloud matching. In particular, we treat it as least squares matching of overlapping 3D surfaces, which are digitized/sampled point by point using a laser scanner device, the photogrammetric method or other surface measurement techniques. Our mathematical model is another generalization of the LSM (Gruen 1985), as for the case of multiple cuboid matching in 3D voxel space (Maas & Gruen 1995).

The details of the mathematical modeling of the proposed method and the execution aspects are explained in the following section. The further extensions to the basic model are given in the third section. Two practical examples for the demonstration of the basic model and the extensions are presented in the fourth section.

2 LEAST SQUARES 3D SURFACE MATCHING (LS3D)

2.1 *The basic estimation model*

Assume that two different partial surfaces of the same object are digitized/sampled point by point, at different times (temporally) or from different viewpoints (spatially). Although the conventional sampling pattern is point based, any other type of sampling pattern is also accepted. $f(x,y,z)$ and $g(x,y,z)$ are discrete 3D representations of the conjugate regions of the object in the *left* and *right* surfaces respectively. The problem statement is estimating the final

location, orientation and shape of the search surface $g(x, y, z)$, which satisfies minimum condition of Least Squares Matching with respect to the template $f(x, y, z)$.

In an ideal situation one would have

$$f(x, y, z) = g(x, y, z) \tag{1}$$

Taking into account the noise and assuming that the template noise is independent of the search noise, Equation 1 becomes

$$f(x, y, z) - e(x, y, z) = g(x, y, z) \tag{2}$$

where $e(x, y, z)$ is a true error vector. Equation 2 are observation equations, which functionally relate the observations $f(x, y, z)$ to the parameters of $g(x, y, z)$. The matching is achieved by least squares minimization of a goal function, which represents the sum of squares of the Euclidean distances between the template and the search surface elements: $\sum \|d\|^2 = \min$, where d stands for the Euclidean distance. The final location is estimated with respect to an initial position of $g(x, y, z)$, the approximation of the conjugate search surface $g^0(x, y, z)$.

To express the geometric relationship between the conjugate surface patches, a 7-parameter 3D similarity transformation is used:

$$\begin{aligned} x &= t_x + m(r_{11}x_0 + r_{12}y_0 + r_{13}z_0) \\ y &= t_y + m(r_{21}x_0 + r_{22}y_0 + r_{23}z_0) \\ z &= t_z + m(r_{31}x_0 + r_{32}y_0 + r_{33}z_0) \end{aligned} \tag{3}$$

where $r_{ij} = \mathbf{R}(\omega,\varphi,\kappa)$ are the elements of the orthogonal rotation matrix, $[t_x\ t_y\ t_z]^T$ is the translation vector, and m is the uniform scale factor. Depending on the deformation between the template and the search surfaces, any other type of 3D transformations could be used, e.g. 12-parameter affine, 24-parameter tri-linear, or 30-parameter quadratic family of transformations.

In order to perform least squares estimation, Equation 2 must be linearized by Taylor expansion.

$$f(x, y, z) - e(x, y, z) = g^0(x, y, z) + \frac{\partial g^0(x, y, z)}{\partial x} \mathrm{d}x + \frac{\partial g^0(x, y, z)}{\partial y} \mathrm{d}y + \frac{\partial g^0(x, y, z)}{\partial z} \mathrm{d}z \tag{4}$$

with

$$\mathrm{d}x = \frac{\partial x}{\partial p_i} \mathrm{d}p_i \quad , \quad \mathrm{d}y = \frac{\partial y}{\partial p_i} \mathrm{d}p_i \quad , \quad \mathrm{d}z = \frac{\partial z}{\partial p_i} \mathrm{d}p_i \tag{5}$$

where $p_i \in \{t_x, t_y, t_z, m, \omega, \varphi, \kappa\}$ is the i-th transformation parameter in Equation 3. Differentiation of Equation 3 gives:

$$\begin{aligned} \mathrm{d}x &= \mathrm{d}t_x + a_{10}\,\mathrm{d}m + a_{11}\,\mathrm{d}\omega + a_{12}\,\mathrm{d}\varphi + a_{13}\,\mathrm{d}\kappa \\ \mathrm{d}y &= \mathrm{d}t_y + a_{20}\,\mathrm{d}m + a_{21}\,\mathrm{d}\omega + a_{22}\,\mathrm{d}\varphi + a_{23}\,\mathrm{d}\kappa \\ \mathrm{d}z &= \mathrm{d}t_z + a_{30}\,\mathrm{d}m + a_{31}\,\mathrm{d}\omega + a_{32}\,\mathrm{d}\varphi + a_{33}\,\mathrm{d}\kappa \end{aligned} \tag{6}$$

where a_{ij} are the coefficient terms, whose expansions are trivial. Using the following notation

$$g_x = \frac{\partial g^0(x, y, z)}{\partial x} \quad , \quad g_y = \frac{\partial g^0(x, y, z)}{\partial y} \quad , \quad g_z = \frac{\partial g^0(x, y, z)}{\partial z} \tag{7}$$

and substituting Equations 6, Equation 4 results in the following:

$$
\begin{aligned}
-e(x,y,z) = {} & g_x\,\mathrm{d}t_x + g_y\,\mathrm{d}t_y + g_z\,\mathrm{d}t_z + (g_x a_{10} + g_y a_{20} + g_z a_{30})\,\mathrm{d}m \\
& + (g_x a_{11} + g_y a_{21} + g_z a_{31})\,\mathrm{d}\omega \\
& + (g_x a_{12} + g_y a_{22} + g_z a_{32})\,\mathrm{d}\varphi \\
& + (g_x a_{13} + g_y a_{23} + g_z a_{33})\,\mathrm{d}\kappa - (f(x,y,z) - g^0(x,y,z))
\end{aligned}
\tag{8}
$$

In the context of the Gauss-Markoff model, each observation is related to a linear combination of the parameters, which are variables of a deterministic unknown function. The terms $\{g_x, g_y, g_z\}$ are numeric first derivatives of this function $g(x,y,z)$.

Equation 8 gives in matrix notation

$$
-\boldsymbol{e} = \mathbf{A}\boldsymbol{x} - \boldsymbol{l} \quad , \quad \mathbf{P} \tag{9}
$$

where $\mathbf{A}$ is the design matrix, $\boldsymbol{x}^{\mathrm{T}} = [\mathrm{d}t_x\ \mathrm{d}t_y\ \mathrm{d}t_z\ \mathrm{d}m\ \mathrm{d}\omega\ \mathrm{d}\varphi\ \mathrm{d}\kappa]$ is the parameter vector, and $\boldsymbol{l} = f(x,y,z) - g^0(x,y,z)$ is the constant vector that consists of the Euclidean distances between the template and correspondent search surface elements. The template surface elements are approximated by the data points, on the other hand the search surface elements are represented in two different kind of piecewise forms (planar and bi-linear) optionally, which will be explained in the following. In general both surfaces can be represented in any kind of piecewise form.

With the statistical expectation operator $\mathrm{E}\{\}$ and the assumptions $\boldsymbol{e} \sim \mathrm{N}(0, \sigma_0^2 \mathbf{Q}_{ll})$ and $\sigma_0^2 \mathbf{Q}_{ll} = \sigma_0^2 \mathbf{P}_{ll}^{-1} = \mathbf{K}_{ll} = \mathrm{E}\{\boldsymbol{e}\boldsymbol{e}^{\mathrm{T}}\}$ Equation 9 is a Gauss-Markoff estimation model. $\mathbf{Q}_{ll}$, $\mathbf{P} = \mathbf{P}_{ll}$ and $\mathbf{K}_{ll}$ stand for *a priori* cofactor, weight and covariance matrices respectively.

The unknown transformation parameters are treated as stochastic quantities using proper *a priori* weights. This extension gives advantages of control over the estimating parameters. We introduce the additional observation equations on the system parameters as

$$
-\boldsymbol{e}_b = \mathbf{I}\boldsymbol{x} - \boldsymbol{l}_b \quad , \quad \mathbf{P}_b \tag{10}
$$

where $\mathbf{I}$ is the identity matrix, $\boldsymbol{l}_b$ is the (fictitious) observation vector for the system parameters, and $\mathbf{P}_b$ is the associated weight coefficient matrix. The weight matrix $\mathbf{P}_b$ has to be chosen appropriately, considering a priori information of the parameters. An infinite weight value ($(\mathbf{P}_b)_{ii} \to \infty$) excludes the i-th parameter from the system, assigning it as constant, whereas zero weight ($(\mathbf{P}_b)_{ii} = 0$) allows the i-th parameter to vary freely, assigning it as unknown parameter in the classical meaning.

The least squares solution of the joint system Equations 9 and 10 gives as the Generalized Gauss-Markoff model the unbiased minimum variance estimation for the parameters

$$
\hat{\boldsymbol{x}} = (\mathbf{A}^{\mathrm{T}}\mathbf{P}\mathbf{A} + \mathbf{P}_b)^{-1}(\mathbf{A}^{\mathrm{T}}\mathbf{P}\boldsymbol{l} + \mathbf{P}_b\boldsymbol{l}_b) \qquad \text{(solution vector)} \tag{11}
$$

$$
\hat{\sigma}_0^2 = (\boldsymbol{v}^{\mathrm{T}}\mathbf{P}\boldsymbol{v} + \boldsymbol{v}_b^{\mathrm{T}}\mathbf{P}_b\boldsymbol{v}_b)/r \qquad \text{(variance factor)} \tag{12}
$$

$$
\boldsymbol{v} = \mathbf{A}\hat{\boldsymbol{x}} - \boldsymbol{l} \qquad \text{(residuals vector for surface observations)} \tag{13}
$$

$$
\boldsymbol{v}_b = \mathbf{I}\hat{\boldsymbol{x}} - \boldsymbol{l}_b \qquad \text{(residuals vector for parameter observations)} \tag{14}
$$

where ^ stands for the Least Squares Estimator, and r is the redundancy. When the system converges, the solution vector converges to zero ($\hat{\boldsymbol{x}} \to 0$). Then the residuals of the surface observations $(\boldsymbol{v})_i$ become the final Euclidean distances between the estimated search surface and the template surface elements.

$$
(\boldsymbol{v})_i = \hat{g}(x,y,z)_i - f(x,y,z)_i \quad , \quad i = \{1,\ldots,n\} \tag{15}
$$

The function values $g^0(x,y,z)$ in Equation 2 are actually stochastic quantities. This fact is neglected here to allow for the use of the Gauss-Markoff model and to avoid unnecessary complications, as typically done in LSM (Gruen 1985).

Since the functional model is non-linear, the solution is obtained iteratively. In the first iteration the initial approximations for the parameters must be provided: $p_i^0 \in \{t_x^0, t_y^0, t_z^0, m^0, \omega^0, \varphi^0, \kappa^0\}$. After the solution vector (Equation 11) is solved, the search surface $g^0(x,y,z)$ is transformed to a new state using the updated set of transformation parameters,

and the design matrix **A** and the discrepancies vector $\boldsymbol{l}$ are re-evaluated. The iteration stops if each element of the alteration vector $\hat{\boldsymbol{x}}$ in Equation 11 falls below a certain limit:

$$\left|\mathrm{d}\,p_i\right| < c_i \quad , \quad \mathrm{d}\,p_i \in \{\mathrm{d}\,t_x, \mathrm{d}\,t_y, \mathrm{d}\,t_z, \mathrm{d}\,m, \mathrm{d}\,\omega, \mathrm{d}\,\varphi, \mathrm{d}\,\kappa\} \tag{16}$$

The numerical derivative terms $\{g_x, g_y, g_z\}$ are defined as local surface normals $\boldsymbol{n}$. Their calculation depends on the analytical representation of the search surface elements.

Two first degree C^0 continuous surface representations are implemented: triangle mesh form (Fig. 1a), which gives planar surface elements, and optionally grid mesh form (Fig. 1b), which gives bi-linear surface elements. The derivative terms are given as *x*-*y*-*z* components of the local normal vectors: $[g_x\ g_y\ g_z]^{\mathrm{T}} = \boldsymbol{n} = [n_x\ n_y\ n_z]^{\mathrm{T}}$.

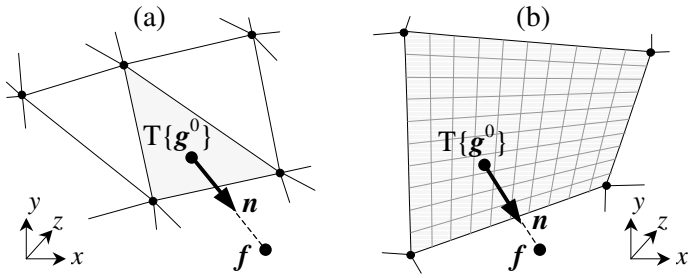

Figure 1. Representation of surface elements in planar (a), and bi-linear (b) forms. Note that T{ } stands for the transformation operator, and $\boldsymbol{g}^0 = g^0(x, y, z)$, $\boldsymbol{f} = f(x, y, z)$.

Basically derivative terms $\{g_x, g_y, g_z\}$ constitute a normal vector field with unit magnitude $\|\boldsymbol{n}\| = 1$ on the search surface. This vector field slides over the template surface towards the final solution, minimizing the least squares objective function.

2.2 *Execution aspects*

The standard deviations of the estimated transformation parameters and the correlations between themselves may give useful information concerning the stability of the system and quality of the data content (Gruen 1985):

$$\hat{\sigma}_p = \hat{\sigma}_0 \sqrt{q_{pp}} \quad , \quad q_{pp} \in \mathbf{Q}_{xx} = (\mathbf{A}^{\mathrm{T}}\mathbf{P}\mathbf{A} + \mathbf{P}_b)^{-1} \tag{17}$$

where $\mathbf{Q}_{xx}$ is the cofactor matrix for the estimated parameters.

In order to localize and eliminate the occluded parts and the outliers a simple weighting scheme adapted from the Robust Estimation Methods is used:

$$(\mathbf{P})_{ii} = \begin{cases} 1 & \text{if} \quad |(\boldsymbol{v})_i| < K\sigma_0 \\ 0 & \text{else} \end{cases} \tag{18}$$

In our experiments K is selected as >10, since it is aimed to suppress only the large outliers. Because of the high redundancy of a typical data arrangement, a certain amount of occlusions and/or smaller outliers do not have significant effect on the estimated parameters.

The computational effort increases with the number of points in the matching process. The main portion of the computational complexity is to search the corresponding elements of the template surface on the search surface, whereas the parameter estimation part is a small system, and can quickly be solved using Cholesky decomposition followed by back-substitution. Searching the correspondence is guided by an efficient boxing structure (Chetverikov 1991), which partitions the search space into cuboids. For a given surface element, the correspondence is searched only in the box containing this element and in the adjacent boxes.

Since the method needs initial approximations of the parameters due to the non-linear functional model, one of the methods for pre-alignment in the literature (Murino et al. 2001, Lucchese et al. 2002, Vanden Wyngaerd & Van Gool 2002) can be utilized.

Two first degree C^0 continuous surface representations are implemented. In the case of multi-resolution data sets, in which point densities are significantly different on the template and search surfaces, higher degree C^1 continuous composite surface representations, e.g. bi-cubic Hermit surface (Peters 1974), should give better results, of course increasing the computational expense.

3 FURTHER EXTENSIONS TO THE BASIC MODEL

3.1 *Simultaneous multi-subpatch matching*

The basic estimation model can be implemented in a multi-patch mode, that is the simultaneous matching of two or more search surfaces $g_i(x, y, z)$, i=1,…,k to one template surface $f(x, y, z)$.

$$-\boldsymbol{e}_i = \mathbf{A}_i \boldsymbol{x}_i - \boldsymbol{l}_i \quad , \quad \mathbf{P}_i \tag{19}$$

Since the parameter vectors $\boldsymbol{x}_1$,…, $\boldsymbol{x}_k$ do not have any joint components, the sub-systems of Equation 19 are orthogonal to each other. In the presence of auxiliary information those sets of equations could be connected via functional constraints, e.g. as in the Geometrically Constrained Multiphoto Matching (Gruen 1985, Gruen & Baltsavias 1988) or via appropriate formulation of multiple (>2) overlap conditions.

An ordinary point cloud includes enormously redundant information. A straightforward way to register such two point clouds could be matching of the whole overlapping areas. This is computationally expensive. We propose multi-subpatch mode as a further extension to the basic model, which is capable of simultaneous matching of sub-surface patches, which are selected in cooperative surface areas. They are joined to the system by the same transformation parameters. This leads to the observation equations

$$-\boldsymbol{e}_i = \mathbf{A}_i \boldsymbol{x} - \boldsymbol{l}_i \quad , \quad \mathbf{P}_i \tag{20}$$

with i=1,…, k subpatches. They can be combined as in Equation 9, since the common parameter vector $\boldsymbol{x}$ joints them to each other. The individual subpatches may not include sufficient information for the matching of whole surfaces, but together they provide a computationally effective solution, since they consist of only relevant information rather than using the full data set. One must carefully select the distribution and size of the subpatches in order to get a homogeneous quality of the transformation parameters in all directions of the 3D space.

3.2 *Simultaneous matching of surface geometry and intensity*

In case of lack of sufficient geometric information (homogeneity or isotropicity of curvatures) the procedure may fail, since there is not a unique solution geometrically, e.g. in case of matching of two planes or spherical objects. An object surface may have some attribute information attached to it. Intensity, color, and temperature are well known examples. Most of the laser scanners can supply intensity information in addition to the Cartesian coordinates for each point, or an additional camera may be used to collect texture. We propose another further extension that can simultaneously match intensity information and geometry under a combined estimation model. In this approach the intensity image of the point cloud also contributes observation equations to the system, considering the intensities as supplementary information to the range image.

Rather than adopting a feature-based or step-wise approach our method sets up quasi-surfaces from intensity information in addition to the actual surfaces. A hypothetical example of forming the quasi-surfaces is given in Figure 2. The procedure starts with the calculation of surface normal vectors at each data point. The actual surface will include noise and surface spikes (Fig. 2b), which lead to unrealistic calculation for the normal vectors. To cope with the problem a moving average or median type filtering process could be employed. But still some noise would remain depending on the window size.

An optimum solution is the least squares fitting of a global trend surface to the whole point cloud (Fig. 2c). It will suppress the noise component and preserves the global continuity of the normal vectors along the surface. We opt for the parametric bi-quadratic trend surface, which is sufficient to model the quadric type of surfaces, e.g. plane, sphere, ellipsoid, etc. For the template surface $f(x, y, z)$ we may write:

$$F(u, w) = \sum_{i=0}^{2} \sum_{j=0}^{2} \boldsymbol{b}_{ij} u^i w^j \tag{21}$$

where $u, w \in [0,1]^2$, $F(u,w) \in \mathbb{R}^3$ is the position vector of any point on the trend surface, and $\boldsymbol{b}_{ij} \in \mathbb{R}^3$ are the algebraic coefficients, which are estimated by the least squares fitting. For each point the normal vector $\boldsymbol{n}_f$ is calculated on the trend surface $F(u,w)$ and attached to the actual surface $f(x, y, z)$ (Fig. 2d):

$$\boldsymbol{n}_f = \boldsymbol{n}_f(u, w) = \boldsymbol{F}_u \times \boldsymbol{F}_w \Big/ \left\| \boldsymbol{F}_u \times \boldsymbol{F}_w \right\| \tag{22}$$

where $\boldsymbol{F}_u$ and $\boldsymbol{F}_w$ are the tangent vectors along the u and w-axes respectively. Finally the quasi-surface $f_c(x, y, z)$ is formed in such a way that each point of the actual surface $f(x, y, z)$ is mapped along its normal vector $\boldsymbol{n}_f$ up to a distance proportional to its intensity value c_f (Fig. 2e).

$$f_c(x, y, z) = f(x, y, z) + \boldsymbol{n}_f \lambda c_f \tag{23}$$

where λ is an appropriate scalar factor for the conversion from the intensity range to the Cartesian space.

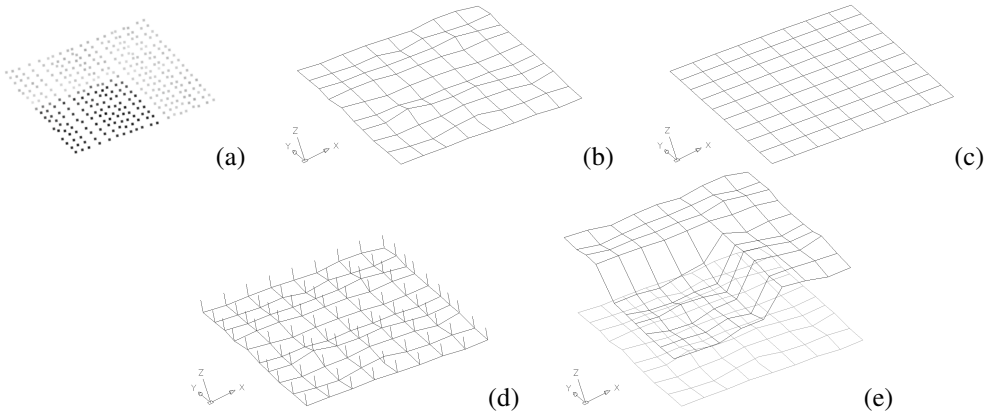

Figure 2. Forming the quasi-surface. (a) Point cloud with intensity information, (b) meshed surface of the point cloud, (c) trend surface fitted to the point cloud, (d) noise-free normal vectors, (e) generated quasi-surface in addition to the actual one.

Rather than the actual surface $f(x, y, z)$ the trend surface $F(u,w)$ can also be defined as the datum, which leads to

$$f_c(x, y, z) = F(u, w) + \boldsymbol{n}_f \lambda c_f \tag{24}$$

This isolates the geometric noise component from the quasi-surface $f_c(x, y, z)$, but strongly smoothes the geometry. Equations 23 and 24 assume a fairly simplistic radiometric model (intensities are mapped perpendicular to the geometric surface). We will refine this model in subsequent work.

The same procedure is performed for the search surface $g(x, y, z)$ as well:

$$g_c(x, y, z) = g(x, y, z) + \boldsymbol{n}_g \lambda c_g \tag{25}$$

Equation 2 should also be valid for the quasi-surfaces under the assumption that similar illumination conditions exist for the both template and search surfaces:

$$f_c(x, y, z) - e_c(x, y, z) = g_c(x, y, z) \tag{26}$$

The random errors of the template and search quasi-surfaces are assumed to be uncorrelated. The contrast and brightness differences or in the extreme case specular reflection will cause model errors, and deteriorate the reliability of the estimation. The radiometric variations between the template and search surface intensities should be adapted before matching by preprocessing or appropriate modeling in the estimation process by extra parameters.

For two images of an object acquired by an optical-passive sensor, e.g. a CCD camera, such an intensity transfer function ($c_f = r_0 + c_g r_1$) could be suitable for the radiometric adaptation, where r_0 (shift) and r_1 (scale) are radiometric correction parameters. In the case of laser scanner derived intensity images the radiometric variations are strongly dependent on both the incident angle of the signal path with respect to object surface normal and object-to-sensor distance. Then, for a plane type of object the radiometric variations can be modeled in first approximating as in the following:

$$f_c(x, y, z) - e_c(x, y, z) = g_c(x, y, z) + r_0 + ur_1 \tag{27}$$

where u is the abscissa of the search trend surface $G(u,w)$, considering that u-axis is the horizontal direction. In other words, u-axis is the principal direction of changing of the incident angles. Depending on the characteristics of scan data it can be replaced by ordinate value w, or another type of parameterization. In general a second order bivariate polynomial ($r_0 + ur_1 + wr_2 + uwr_3 + u^2 r_4 + w^2 r_5$) or an appropriate subpart of it can be used.

Although the radiometric parameters r_0 and r_1 are linear *a priori*, we expand them to Taylor series. Equation 27 in linearized form gives:

$$\begin{aligned} -e_c(x, y, z) = {} & g_{cx}\,\mathrm{d}x + g_{cy}\,\mathrm{d}y + g_{cz}\,\mathrm{d}z \\ & + \mathrm{d}r_0 + u\,\mathrm{d}r_1 - (f_c(x, y, z) - (g_c^0(x, y, z) + \{r_0^0 + ur_1^0; \boldsymbol{n}_g\})) \end{aligned} \tag{28}$$

where g_{cx}, g_{cy}, and g_{cz} stand for the derivative terms like as given in Equation 7 for the actual surface observations. The first approximations of the radiometric parameters are $r_0^0 = \mathrm{r}_1^0 = 0$. At the end of the each iteration the quasi search surface $g_c^0(x, y, z)$ is transformed to a new state using the updated set of transformation parameters, and subsequently re-shaped by the current set of radiometric parameters $r_0^0 + ur_1^0$ along the normal vectors $\boldsymbol{n}_g$, which are calculated on the search trend surface $G(u,w)$.

The quasi-surfaces are treated like actual surfaces in the estimation model. They contribute observation equations to the design matrix, joining the system by the same set of transformation parameters. After the further expansion of Equation 28 and with the assumptions $\mathrm{E}\{\boldsymbol{e}_c\} = 0$ and $\mathrm{E}\{\boldsymbol{e}_c \boldsymbol{e}_c^{\mathrm{T}}\} = \sigma_0^2 \mathbf{P}_c^{-1}$, the total system becomes

$$\begin{aligned} -\boldsymbol{e} &= \mathbf{A}\boldsymbol{x} - \boldsymbol{l} \quad , \ \mathbf{P} \\ -\boldsymbol{e}_b &= \mathbf{I}\boldsymbol{x} - \boldsymbol{l}_b \quad , \ \mathbf{P}_b \\ -\boldsymbol{e}_c &= \mathbf{A}_c \boldsymbol{x} - \boldsymbol{l}_c \quad , \ \mathbf{P}_c \end{aligned} \tag{29}$$

where $\boldsymbol{e}_c$, $\mathbf{A}_c$, and $\mathbf{P}_c$ are the true error vector, the design matrix, and the associated weight coefficient matrix for the quasi-surface observations respectively, and $\boldsymbol{l}_c$ is the constant vector that contains the Euclidean distances between the template and correspondent search quasi-surfaces elements. The hybrid system in Equation 29 is of the *combined adjustment* type that allows simultaneous matching of geometry and intensity.

In our experiments, weights for the quasi-surface observations are selected as $(\mathbf{P}_c)_{ii} < (\mathbf{P})_{ii}$, and the intensity measurements of the (laser) sensor are considered to be uncorrelated with the distance measurements ($\mathrm{E}\{\boldsymbol{e}_c \boldsymbol{e}^{\mathrm{T}}\} = 0$) for the sake of simplicity of the stochastic model.

4 EXPERIMENTAL RESULTS

Two practical examples are given to show the capabilities of the method. All experiments were carried out using own self-developed C/C++ software that runs on Microsoft Windows® OS. The processing times were counted on a PC with Intel® P4 2.53Ghz CPU and 1 GB RAM. In all experiments the initial approximations of the unknowns were provided by interactively selecting 3 common points on both surfaces before matching. Since in all data sets there was no scale difference, the scale factor m was fixed to unity by infinite weight value ($(\mathbf{P}_b)_{ii} \rightarrow \infty$).

The first example is the registration of two point clouds of a room (Fig. 3) in Neuschwanstein Castle in Bavaria, Germany. The scanning was performed by using the IMAGER 5003 (Zoller+Fröhlich) terrestrial laser scanner. The average point spacing is 5 millimeters. The point cloud Figure 3b was matched to Figure 3a by use of the LS3D surface matching. The iteration criteria values c_i were selected as 1.0e-4 meters for the elements of the translation vector and 1.0e-3 grad for the rotation angles.

In this experiment the whole overlapping areas were matched. The numerical result of the matching is given in part I of Table 1. Relatively homogeneous and small magnitudes of the theoretical precision values of the parameters show success of the matching.

(a) (b) (c)

Figure 3. Example “room”. (a) Template and (b) search point clouds, (c) composite point cloud after the LS3D surface matching. Note that laser scanner derived intensities are back-projected onto the point clouds only for the visualization purpose.

A further matching process was carried out using the simultaneous multi-subpatch approach of the LS3D. Seven occlusion-free cooperative subpatches were selected. The result of the matching is given in part II of Table 1. The simultaneous multi-subpatch approach apparently decreases the computation times.

Table 1. Numerical results of “room” example.

#	Surface mode	No. points	Iter.	Time (sec.)	Sigma naught (mm)	Standard dev. of t_x / t_y / t_z (mm)	Standard dev. of ω / φ / κ (grad/100)
I	P	1,155,502	10	142.5	3.69	0.01 / 0.01 / 0.01	0.03 / 0.04 / 0.02
	B		11	209.9	3.70	0.01 / 0.01 / 0.01	0.03 / 0.04 / 0.02
II	P	279,088	8	25.8	3.60	0.01 / 0.02 / 0.03	0.07 / 0.06 / 0.04
	B		11	43.9	3.65	0.01 / 0.02 / 0.03	0.07 / 0.06 / 0.04

P: planar, B: bi-linear surface representation.

The second experiment refers to simultaneous matching of surface geometry and intensity. Two partial scans of a wall painting in Neuschwanstein data set were matched (Fig. 4). Laser scanner derived reflectance values were used as intensity information. The actual surface observations are considered as the unit weight $(\mathbf{P})_{ii} = 1$. Consequently weights for the quasi-surface observations are selected as $(\mathbf{P}_c)_{ii} = 0.75$. The iteration criteria values c_i were selected as 2.0e-4 meters for the elements of the translation vector and 5.0e-3 grad for the rotation angles. The search surface (Fig. 4a) was matched to the template one (Fig. 4b). The numerical results are given in Table 2.

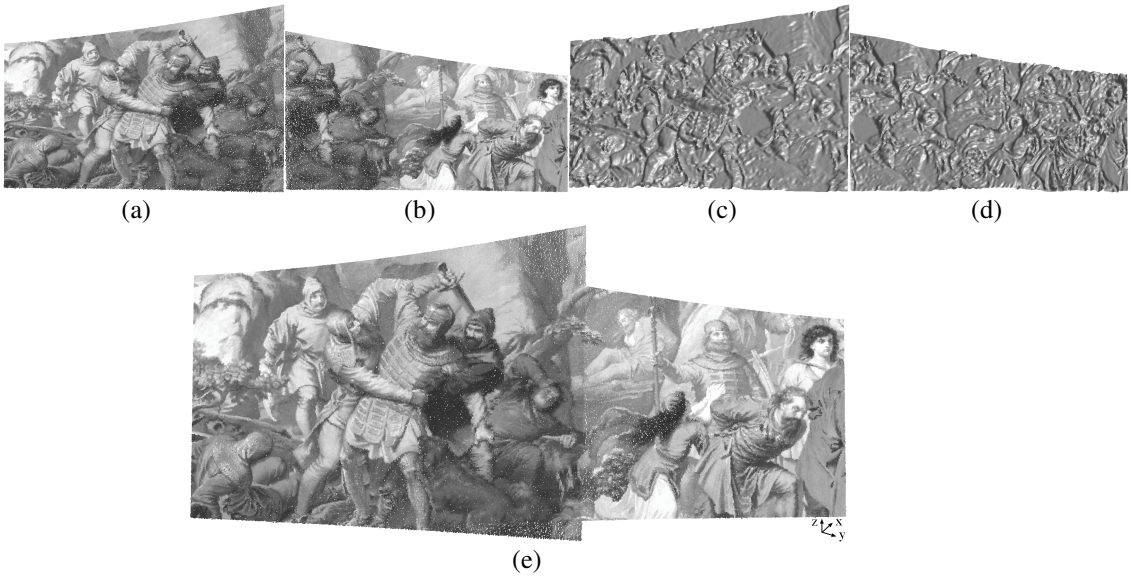

Figure 4. Example "wall painting". Actual (a) search and (b) template surfaces, generated (c) quasi-search and (d) quasi-template surfaces, (e) composite point cloud after the simultaneous matching of geometry and intensity by LS3D. Note that laser scanner derived intensities are back-projected onto the point clouds (a), (b), and (e).

Since the object is a plane, only surface geometry is not enough for the matching. Using the combined matching of surface geometry and intensity approach of the LS3D a successful solution has been achieved. The generated quasi surfaces (Fig. 4c and 4d) have been used in addition to the actual ones (Fig. 4a and 4b) in the matching process. The use of the trend surface as datum gives a slightly better convergence rate.

Table 2. Numerical results of "wall painting" example.

#	Surface mode	No. points	Iter.	RMSE (mm)	Standard dev. of t_x / t_y / t_z (mm)	Standard dev. of ω / φ / κ (grad/100)
III [a]	P	31,859	14	1.67	0.02 / 0.21 / 0.12	0.28 / 0.25 / 0.46
	B		13	1.72	0.02 / 0.21 / 0.12	0.29 / 0.26 / 0.44
IV [b]	P	31,858	13	1.68	0.02 / 0.19 / 0.11	0.25 / 0.23 / 0.41
	B		12	1.73	0.02 / 0.19 / 0.11	0.26 / 0.24 / 0.40

RMSE: root mean square error of the residuals of the actual surface observations.
[a]) datum are the actual surfaces $f/g(x, y, z)$.
[b]) datum are the trend surfaces $F/G(u, w)$.

5 CONCLUSIONS

An algorithm for the least squares matching of overlapping 3D surfaces is presented. Our proposed method, the Least Squares 3D Surface Matching (LS3D), estimates the transformation parameters between two or more fully 3D surfaces, using the Generalized Gauss-Markoff model, minimizing the sum of squares of the Euclidean distances between the surfaces. The mathematical model is a generalization of the least squares image matching method and offers high flexibility for any kind of 3D surface correspondence problem. The least squares concept allows for the monitoring of the quality of the final results by means of precision and reliability criterions. By appropriately selecting the 3D transformation method and the surface representation type, it is able to match multi-resolution, multi-temporal, multi-scale, and multi-sensor data sets.

The capabilities of the technique are illustrated by a practical example. There are several ways to extend the technique. Here we give two of them, which are simultaneous matching of surface geometry and intensity under a combined estimation model and simultaneous multi-subpatch matching. Future studies will include more practical examples to demonstrate the full power of the technique.

The technique can be applied to a great variety of data co-registration problems. Since it reveals the sensor noise level and accuracy potential of any kind of surface measurement method or device, it can be used for comparison and validation studies. In addition time dependent (temporal) variations of the object surface can be inspected, tracked, and localized using the statistical analysis tools of the method.

ACKNOWLEDGEMENTS

The laser scanner data set is courtesy of Zoller+Fröhlich GmbH Elektrotechnik. The author is financially supported by an ETHZ Internal Research Grant, which is gratefully acknowledged.

REFERENCES

Bergevin, R., Soucy, M., Gagnon, H. & Laurendeau, D. 1996. Towards a general multi-view registration technique. *IEEE Trans. on Pattern Analysis and Machine Intelligence* 18(5): 540-547.

Besl, P.J. & McKay, N.D. 1992. A method for registration of 3D shapes. *IEEE Trans. on Pattern Analysis and Machine Intelligence* 14(2): 239-256.

Campbell, R.J. & Flynn, P.J. 2001. A survey of free-form object representation and recognition techniques. *Computer Vision and Image Understanding* 81(2): 166-210.

Chen, Y. & Medioni, G. 1992. Object modelling by registration of multiple range images. *Image and Vision Computing* 10(3): 145-155.

Chetverikov, D. 1991. Fast neighborhood search in planar point sets. *Pattern Recognition Letters* 12(7): 409-412.

Dorai, C., Weng, J. & Jain, A.K. 1997. Optimal registration of object views using range data. *IEEE Trans. on Pattern Analysis and Machine Intelligence* 19(10): 1131-1138.

Ebner, H. & Strunz, G. 1988. Combined point determination using Digital Terrain Models as control information. *International Archives of Photogrammetry & Remote Sensing,* Vol. 27, Part B11/3: 578-587.

Godin, G., Laurendeau, D. & Bergevin, R. 2001. A method for the registration of attributed range images. *Proc. of IEEE Int. Conf. on 3D Digital Imaging and Modeling*, 179-186, Quebec, 28 May – 1 June 2001.

Gruen, A. 1985. Adaptive least squares correlation: a powerful image matching technique. *South African Journal of Photogrammetry, Remote Sensing and Cartography* 14(3): 175-187.

Gruen, A. & Baltsavias, E.P. 1988. Geometrically Constrained Multiphoto Matching. *Photogrammetric Engineering & Remote Sensing* 54(5): 633-641.

Gruen, A. 1996. Least squares matching: a fundamental measurement algorithm. In K.B. Atkinson (Ed.), *Close Range Photogrammetry and Machine Vision*: 217-255. Caithness (UK): Whittles.

Johnson, A.E. & Kang S.B. 1999. Registration and integration of textured 3D data. *Image and Vision Computing* 17(2): 135-147.

Jokinen, O. & Haggren, H. 1998. Statistical analysis of two 3-D registration and modeling strategies. *ISPRS Journal of Photogrammetry & Remote Sensing* 53(6): 320-341.

Lucchese, L., Doretto, G. & Cortelazzo, G.M. 2002. A frequency domain technique for range data registration. *IEEE Trans. on Pattern Analysis and Machine Intelligence* 24(11): 1468-1484.

Maas, H.G. & Gruen, A. 1995. Digital photogrammetric techniques for high resolution three dimensional flow velocity measurements. *Optical Engineering* 34(7): 1970-1976.

Maas, H.G. 2002. Methods for measuring height and planimetry discrepancies in airborne laserscanner data. *Photogrammetric Engineering & Remote Sensing* 68(9): 933-940.

Masuda, T. & Yokoya, N. 1995. A robust method for registration and segmentation of multiple range images. *Computer Vision and Image Understanding* 61(3): 295-307.

Murino, V., Ronchetti, L., Castellani, U. & Fusiello, A. 2001. Reconstruction of complex environments by robust pre-aligned ICP. *Proc. of IEEE Int. Conf. on 3D Digital Imaging and Modeling*, 187-194, Quebec, 28 May – 1 June 2001.

Neugebauer, P.J. 1997. Reconstruction of real-world objects via simultaneous registration and robust combination of multiple range images. *International Journal of Shape Modeling* 3(1-2): 71-90.

Okatani, I.S. & Deguchi, K. 2002. A method for fine registration of multiple view range images considering the measurement error properties. *Computer Vision and Image Understanding* 87(1-3): 66-77.

Peters, G.J. 1974. Interactive computer graphics application of the parametric bi-cubic surface to engineering design problems. In R. Barnhill & R. Riesenfeld (Eds.), *Computer Aided Geometric Design*: 259-302. New York: Academic Press.

Postolov, Y., Krupnik, A. & McIntosh, K. 1999. Registration of airborne laser data to surfaces generated by Photogrammetric means. *International Archives of Photogrammetry & Remote Sensing*, Vol. 32, Part 3/W14: 95-99.

Potmesil, M. 1983. Generating models of solid objects by matching 3D surface segments. *Int. Joint Conference on Artificial Intelligence*: 1089-1093, Karlsruhe, 8-12 August 1983.

Rosenholm, D. & Torlegard, K. 1988. Three-dimensional absolute orientation of stereo models using Digital Elevation Models. *Photogrammetric Engineering & Remote Sensing* 54(10): 1385-1389.

Roth, G. 1999. Registering two overlapping range images. *Proc. of IEEE Int. Conf. on 3D Digital Imaging and Modeling*: 191-200, Ottawa, 4-8 October 1999.

Rusinkiewicz, S. & Levoy, M. 2001. Efficient variants of the ICP algorithm. *Proc. of IEEE Int. Conf. on 3D Digital Imaging and Modeling*: 145-152, Quebec, 28 May – 1 June 2001.

Szeliski, R. & Lavallee, S. 1996. Matching 3-D anatomical surfaces with non-rigid deformations using octree-splines. *International Journal of Computer Vision* 18(2): 171-186.

Vanden Wyngaerd, J. & Van Gool, L. 2002. Automatic crude patch registration: towards automatic 3D model building. *Computer Vision and Image Understanding* 87 (1-3): 8-26.

Vanden Wyngaerd, J. & Van Gool, L. 2003. Combining texture and shape for automatic crude patch registration. *Proc. of IEEE Int. Conf. on 3D Digital Imaging and Modeling*: 179-186, Banff, 6-10 October 2003.

Weik, S. 1997. Registration of 3-D partial surface models using luminance and depth information. *Proc. of IEEE Int. Conf. on 3DIM*: 93-100, Ottawa, 12-15 May 1997.

Williams, J.A., Bennamoun, M. & Latham, S. 1999. Multiple view 3D registration: A review and a new technique. *Proc. of IEEE Int. Conference on Systems, Man, and Cybernetics*: 497-502, Tokyo, 12-15 October 1999.

Yoshida, K. & Saito, H. 2002. Registration of range images using texture of high-resolution color images. *Proc. of IAPR Workshop on Machine Vision Applications (MVA'02)*: 150-153, Nara, 11-13 December 2002.

Zhang, Z. 1994. Iterative point matching for registration of free-form curves and surfaces. *International Journal of Computer Vision* 13(2): 119-152.